Journal of Hydrology 570 (2019) 473–485

Contents lists available at ScienceDirect

Journal of Hydrology

journal homepage: www.elsevier.com/locate/jhydrol

Research papers

Climate change uncertainties in seasonal drought severity-area-frequency curves: Case of arid region of Pakistan

Kamal Ahmed[a,b,*], Shamsuddin Shahid[b], Eun-Sung Chung[c], Xiao-jun Wang[d,e], Sobri Bin Harun[b]

[a] Faculty of Water Resource Management, Lasbela University of Agriculture, Water and Marine Sciences, Balochistan, Pakistan
[b] Faculty of Civil Engineering, Universiti Teknologi Malaysia (UTM), 81310 Johor Bahru, Malaysia
[c] Department of Civil Engineering, Seoul University of Science and Technology, Seoul 01811, Republic of Korea
[d] State Key Laboratory of Hydrology-Water Resources and Hydraulic Engineering, Nanjing Hydraulic Research Institute, Nanjing 210029, China
[e] Research Center for Climate Change, Ministry of Water Resources, Nanjing 210029, China

ARTICLE INFO

This manuscript was handled by Andras Bardossy, Editor-in-Chief, with the assistance of Antonino Cancelliere, Associate Editor

Keywords:
Seasonal drought
Severity-area-frequency
CMIP5
RCPs
Statistical downscaling
Arid region

ABSTRACT

The uncertainty assessment of the changes in drought characteristics due to climate change has caught the attention of the scientific community. This study used gauge-based gridded precipitation data obtained from Global Precipitation Climatology Centre (GPCC) to reconstruct historical droughts and downscale future precipitation projected by seven general circulation models (GCMs) of Coupled Model Inter-comparison Project phase 5 (CMIP5) under four Representative Concentration Pathways (RCP) scenarios, namely, RCP2.6, RCP4.5, RCP6.0 and RCP8.5. Support vector machine (SVM) and quantile mapping were used for downscaling and GCM bias correction, respectively. The model performances were assessed based on statistical measures. The historical and future projected precipitation data were finally used to characterize the seasonal droughts using Standardized Precipitation Index (SPI) for different crop growing periods. The drought severity-area-frequency (SAF) curves for the historical (1961–2010) and three future periods (2010–2039, 2040–2069, and 2070–2099) were developed. The uncertainty band of future drought SAF curves was estimated using Bayesian bootstrap (BB) at a 95% confidence level. As a result, SVM was successful in downscaling the precipitation of all selected CMIP5 GCMs. The seasonal ensemble of GCMs projected an increase in precipitation ranging from 8% to 41% under all scenarios. The historical SAF curves revealed that for equal drought severity, larger areas are affected by droughts having higher return periods. Future projections of droughts revealed the increase in affected area for lower severity and return period droughts and the decrease for higher severity and return period droughts. The uncertainty bands of drought SAF curves with higher return periods were found much wider compared to those with lower return periods which indicates more uncertainty in the projection of higher severity and return period droughts.

1. Introduction

Drought is likely to become more recurrent and severe in future and can have severe and long-lasting impacts on natural and human systems (Nam et al., 2015; Rahmat et al., 2016; Touma et al., 2015). Droughts can be more acute for semi-arid and arid regions (Forouzani and Karami, 2010; Liu and Hwang, 2015). The situation can become much worse in the semi-arid countries like Pakistan, where the economy is mainly based on agriculture (Kazmi et al., 2015; Miyan, 2015). Drought is a common phenomenon in Pakistan, which occurs at least thrice every ten years (Anjum et al., 2012). The country has experienced a number of severe droughts in recent history, which were mainly confined to Sindh and Balochistan provinces of Pakistan (Ashraf and Routray, 2015). Balochistan province covers 44% of the total land of Pakistan faced severe droughts in 1967–1969, 1971, 1973–1975, 1994 and 1998–2002 (Ahmed et al., 2015). The prolonged drought in 1998–2002 reduced crop yields by 60–80% that resulted in severe negative impacts on the economy of the province as well as the whole country (Sarwar, 2008). There is a growing concern in recent years on increasing severity and frequency of droughts in Pakistan like in many other parts of Asia (Ahmed et al., 2015; Wang et al., 2012). Zahid and Rasul (2012) reported a significant increase in heat waves frequency over Balochistan, which indicates the possibility of more frequent drought in the future. Therefore, it is important to understand the possible changes in future drought characteristics for climate change adaptation and mitigation planning.

* Corresponding author at: Faculty of Civil Engineering, Universiti Teknologi Malaysia (UTM), 81310 Johor Bahru, Malaysia.
E-mail address: kamal_brc@hotmail.com (K. Ahmed).

https://doi.org/10.1016/j.jhydrol.2019.01.019
Received 6 February 2017; Received in revised form 18 October 2018; Accepted 4 January 2019
Available online 19 January 2019

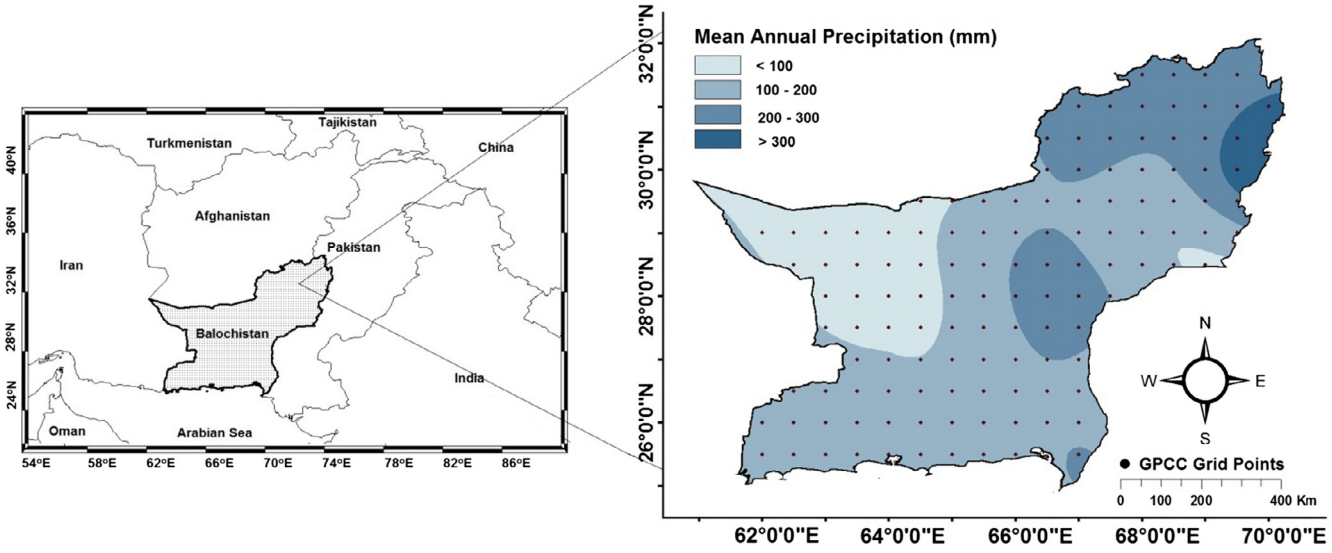

Fig. 1. Location and annual mean precipitation map of Balochistan province, Pakistan.

Several studies (Swain and Hayhoe, 2015; Touma et al., 2015; Wang and Chen, 2014; Wang et al., 2014; Zarch et al., 2015) have been conducted in recent years to project future changes in droughts using Coupled Model Intercomparison Project Phase 5 (CMIP5) general circulation model (GCMs) data. However, most studies characterized droughts without giving any indication of drought risk during different seasons or cropping periods. Droughts are found to be significantly damaging when they coincide with cropping seasons (Mishra and Cherkauer, 2010). Thus, it is very important to predict future droughts during cropping seasons to mitigate the impacts in the context of climate change.

The GCMs used for projecting future climate introduce uncertainties in projections. Therefore, it is obvious that drought characterization based on GCM projections contains uncertainties. Exploring uncertainties and providing reliable information is a major challenge in climate change research (Kim et al., 2015). As the GCM configuration is the main source of uncertainty in climate projections, ensembles of GCM projections are used to incorporate uncertainties in impact assessment. Two main approaches used to assess climate change uncertainties in droughts are perturbed-physics ensembles i.e. projections from different parameterizations of the same model (Burke and Brown, 2010; Taylor et al., 2013) and multi-model ensembles (Burke and Brown, 2008; Dai and Zhao, 2016; Mishra and Singh, 2009; Vidal and Wade, 2009). The improvements in CMIP5 models such as the availability of a large number of projections at higher resolution and better representation of Earth system processes have provided greater confidence in climate change projections and opportunity to assess uncertainty using multi-model ensemble (Knutti and Sedláček, 2013).

The drought severity-area-frequency (SAF) curves (Henriques and Santos, 1999) quantitatively relate the values of drought severity, areal extent and return period and therefore, widely used to represent all characteristics of droughts together (Loukas and Vasiliades, 2004; Rajsekhar et al., 2015). Mishra and Singh (2009) argued that high uncertainties in the GCM structure and complexities in droughts have made event-based drought analysis difficult. Therefore, analysis of future changes in droughts based on SAF curves is preferred over the event-based drought. Some studies (Burke and Brown, 2010; Lee and Kim, 2013; Mishra and Singh, 2009) considered the uncertainties in future projections of droughts, however none of them has assessed the uncertainty within the SAF curve. This study quantified the uncertainty within the SAF curves using Bayesian theorem and Bootstrap resampling technique (Efron, 1992; Rubin, 1981). The technique has been recommended to evaluate uncertainty in hydrological or climate models (Hu et al., 2015).

The main aim of the present study was to investigate the impacts of climate change on SAF curves for the historical and future droughts during four climatic seasons namely early winter (November–January), late winter (February–April), early summer (May–July), and late summer (August–October); and the two major cropping seasons, Kharif (May–October) and Rabi (November–April) in Pakistan. The gauge-based gridded precipitation data provided by the Global Precipitation Climatology Centre (GPCC) of the Deutscher Wetterdienst (Becker et al., 2013) having a resolution of at $0.5^{\circ} \times 0.5^{\circ}$ and seven GCMs participating in CMIP5 were used for this purpose. Support Vector Machine (SVM) was used to downscale coarse resolution GCM precipitation to GPCC scale and Quantile mapping (QM) was used to correct the bias in GCMs. Standardized Precipitation Index (SPI) (McKee et al., 1993) was used to characterize seasonal droughts. The return periods of various severities of droughts were interpolated to derive the SAF curves of seasonal droughts for the historical (1961–2010) and three future periods (2010–2039, 2040–2069, and 2070–2099).

2. Study area and datasets

2.1. Study area

Balochistan is situated in the southwestern part of Pakistan (Fig. 1). The province is the homeland of around 8.5 million people with a population density of 23 people per km^2 (GoB, 2014). The province is the largest region covering an area of 347,000 km^2, constituting 44% of the total mass of Pakistan. More than 85% of the population in the province depends on agriculture for their livelihood (Ashraf et al., 2014). Agriculture and livestock sectors play a vital role in the economy and employ about 67% of the labor force (Hussein, 2004).

Precipitation in the area varies from 30 mm/yr in the southwest desert to 397 mm/yr in the northeast (Fig. 1). Overall, the precipitation climatology is divided into, (1) Early Winter (November – January); (2) Late Winter (February – April); (3) Early Summer (May – July); and (4) Late Summer (August – October) (Ahmed et al., 2015; Snead, 1968). Majority of the area belongs to the arid climate followed by hyper-arid and semi-arid (Fig. 2a). The topography of the study area presented in Fig. 2b revealed terrain is primarily dominated by mountains. The mountains are the eastern extension of the Iranian plateau, subdivided by moderately high to high mountain ranges running roughly north-south and extended to the Himalaya system (Verheijen, 1998). Highest mountains are located in the northern and central parts of the province.

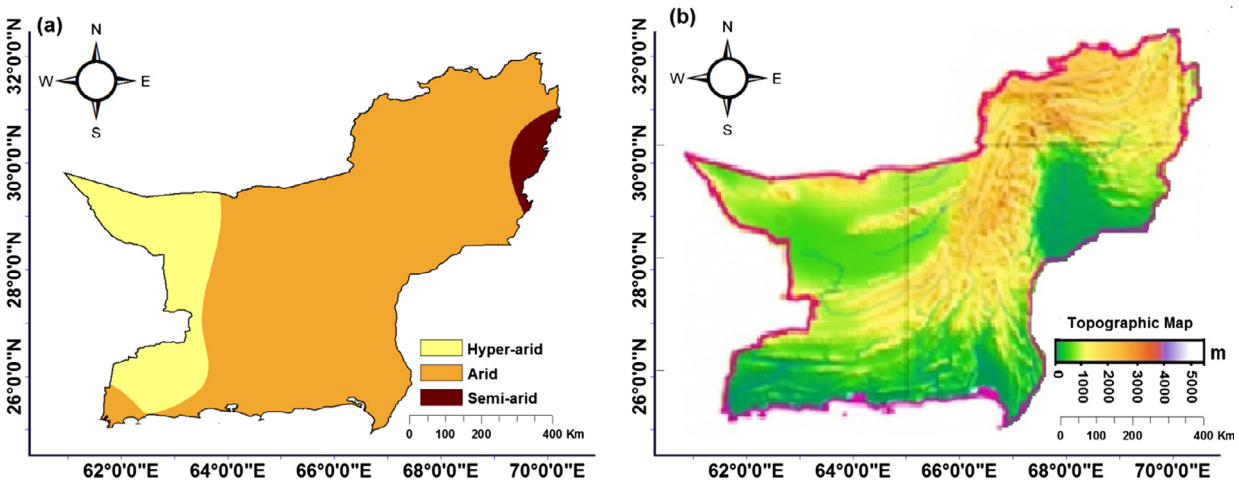

Fig. 2. Map of (a) aridity; and (b) topography of Balochistan.

The harsh climate and rough terrain of the province have limited the cultivation activities, leaving most of the area to be used as rangeland grazing (Naz Mirza et al., 2009). The rangeland in the province provides around 90% of feed requirement for livestock (Shafiq and Kakar, 2007). Any variation in climate severely affects the agriculture and people's livelihood in this region.

2.2. Datasets

The precipitation dataset provided by GPCC was used as reference data in this study. The GPCC has produced several products at different spatial resolutions (Schneider et al., 2014). In this study, 0.5° spatial resolution full data reanalysis product version 6 from GPCC was used. The GPCC dataset is developed using a large number of observations and it is available over a longer time span (Ahmed et al., 2015; Spinoni et al., 2014). Therefore, it has been widely used for precipitation downscaling and drought assessments (Chen et al., 2014; Mullan et al., 2015; Shirvani and Landman, 2015). The monthly precipitation dataset from 130 grid points covering Balochistan (Fig. 1) for the period 1961–2010 was considered in this study.

The monthly precipitation data of seven CMIP5 GCMs for historical simulations and future projections were selected in this study. The selection criteria of the models were the availability of four RCP scenarios and a model from all countries participating in CMIP5. The RCPs represent four different scenarios of radiative forcing levels namely 2.6, 4.5, 6.0, and 8.5 W/m^2 (Van Vuuren et al., 2011; Winkler and Winiwarter, 2015). Four selected RCPs include a very low forcing level known as mitigation scenario (RCP2.6), two medium forcing level known as stabilization scenarios (RCP4.5/RCP6.0) and one very high forcing level know as very high greenhouse gas emission scenario (RCP8.5). The descriptions of the selected models are given in Table 1. These models are available in different resolutions. Higher resolutions are generally desirable for assessing regional hydro-climate variables while the coarser are preferred over the regions with complex topography and coastlines (Zahid and Iqbal, 2015). Therefore, all selected CMIP5 precipitation simulations are re-gridded onto a common 2° × 2° grid to reduce the biases and cover the high variation in topography and coastlines of the study area.

CMIP5 GCMs have several ensemble members such as r1i1p1, r2i1p1 r3i1p1, r4i1p1 etc. that represent the realization, initialization and physics of the models. In order to have an unbiased comparison among various models, we considered the ensemble, r1i1p1 for the historical period data for 1961–2005 and RCPs data for analyzing four future RCP scenarios for the period 2010–2099.

3. Methodology

3.1. Procedure

The flowchart of the procedure used in this study is shown in Fig. 3. This study was broadly divided into two parts. In the first part, monthly precipitations simulated by seven GCMs were extracted from IPCC CMIP5 data portal. The extracted data were regridded/remapped to a common grid of 2° × 2° by using bilinear interpolation approach in climate data operator environment developed by Max-Planck-Institute for meteorology. The simulated precipitations from CMIP5 models were considered as a model predictor in the downscaling model (Sa'adi et al., 2017). Eden et al. (2012) reported that simulated precipitation is a very good predictor for the true precipitation, and thus can be used as a predictor. Stepwise regression was used to optimally link the GCM simulated precipitations to GPCC precipitation. It allowed the selection of the subset of GCM simulated precipitations that can best predict the GPCC precipitation at a grid point, which was then used for downscaling model development. The downscaling model was trained for 70% and tested for 30% of GPCC data using SVM. The quantile mapping was applied to reduce the biases between the GCM outputs and

Table 1
List of CMIP5 models used in this study.

Institute	Model Name	Resolution (Lat × Lon)
Beijing Climate Center China	BCC-CSM1.1	2.8 x2.8
NASA/GISS (Goddard Institute for Space Studies), USA	GISS-E2-H	2.5 × 2.5
Met Office Hadley Centre, UK	HadGEM2-ES	1.875 × 1.25
Atmosphere and Ocean Research Institute (The University of Tokyo), National Institute for Environmental Studies, and Japan Agency for Marine-Earth Science and Technology, Japan	MIROC-ESM	2.8 × 2.8
Bjerknes Centre for Climate Research, Norwegian Meteorological Institute, Norway	NorESM1-M	2.5 × 1.9
National Institute of Meteorological Research, Korea Meteorological Administration, South Korea	HadGEM2-AO	1.875 × 1.25
Commonwealth Scientific and Industrial Research Organization/Queensland Climate Change Centre of Excellence, Australia	CSIRO-Mk3.6.0	1.861 × 1.875

Source: http://cmip-pcmdi.llnl.gov/cmip5/.

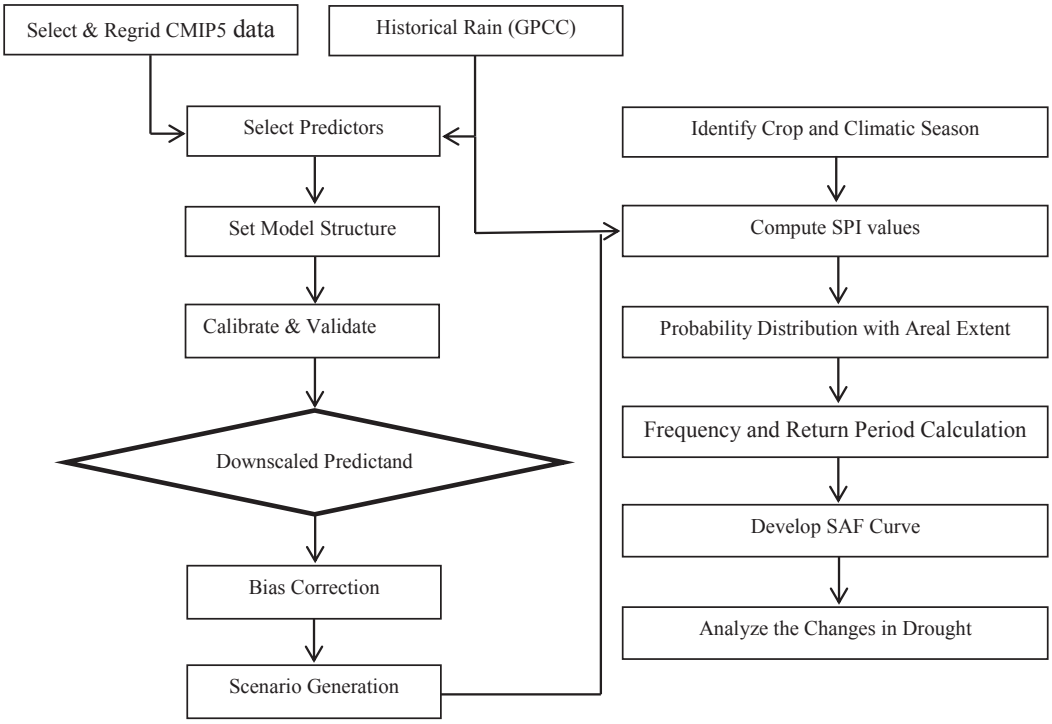

Fig. 3. Procedure used in this study to estimate future SAF curves.

observations. The performances of models were assessed using different model evaluation statistics.

In the second part, droughts during various climatic (3-month SPI) or crop growing seasons (6-month SPI) were reconstructed by estimating SPI at each grid point for the timescale of corresponding seasons. SPI values were arranged in time series for each season to associate with different areal extents. The frequency analysis was performed on drought severities for different areal extents to estimate the return period of associated severity and areal extent for the development of SAF curves. The methods used in this study are discussed below:

3.2. Downscaling and projections

3.2.1. Support vector machines (SVM)

SVM can model highly nonlinear relationships and therefore, widely used in solving non-linear problems (Acton, 2012; Asefa et al., 2004; Dibike et al., 2001; Khadam and Kaluarachchi, 2004). In SVM-based regression, the relationship between predictand (y) with the predictors (x_i) is estimated as follows:

$$y = f(x_i) = w\phi(x_i) + b \tag{1}$$

where w represents weight vector; b represents bias; ϕ represents a nonlinear transfer function that maps the input vectors (x_i) into a high-dimensional feature space.

The SVM solves the nonlinear regression function by optimizing an ε-insensitivity loss function,

$$\frac{1}{2}w^T w + C\sum_{i=1}^{N}\xi_i + C\sum_{i=1}^{N}\xi_i^* \tag{2}$$

The function can be minimized using the following criteria,

$$\left.\begin{aligned} &w^T\phi(x_i) + b - y_i \le \varepsilon + \xi_i^* \\ &y_i - w^T\phi(x_i) - b \le \varepsilon + \xi_i \\ &\xi_i\xi_i^* \ge 0,\ i = 1, 2, \ldots N \end{aligned}\right\} \tag{3}$$

where ξ_i and ξ^*_i denote slack variables which are the distance of the training data set points from the region to an error tolerance ε; and C is a constant.

Eq. (3) can be solved by the Lagrangian multipliers (α_i, α_i^*, η, η^*). Quadratic programing was used for this purpose. After optimization, it can be written as,

$$f(x_i) = \sum_{i=1}^{N}(\alpha_i - \alpha_i^*)\{x_i, x\} + b \tag{4}$$

This Eq. (4) is suitable for solving linear regression problems. It can be extended to nonlinear regression problem that maps the input vectors into a high–dimensional feature space ϕ, which in turn linearize the relationship between input and output. Thus, the Eq. (4) can be written as,

$$f(x_i) = \sum_{i=1}^{N}(\alpha_i - \alpha_i^*)k(x_i, x) + b \tag{5}$$

$$k(x_i x) = \{\phi(x_i), \phi(x)\}$$

where $k(x_i,x)$ is the kernel function.

The performance of the SVM model primarily relies on the optimum selection of model parameters that include kernel type, regularization parameter (C) and epsilon value (ε). In the present study, a k-fold cross-validation was used to find the optimum values of model parameters.

3.2.2. Quantile mapping

QM developed by Panofsky et al. (1958) relies on cumulative distributive function. The principle is to adjust the distribution of model output with the observed data set. Gudmundsson et al. (2012) formulated QM as:

$$P_o = h(P_m) \tag{6}$$

where P_o is observed precipitation, h is a transfer function, and P_m is downscaled precipitation. The distribution of data set and parameters of the distribution are determined and then the following expression is used for bias correction:

$$P_o = F_o^{-1}F_m(P_m) \tag{7}$$

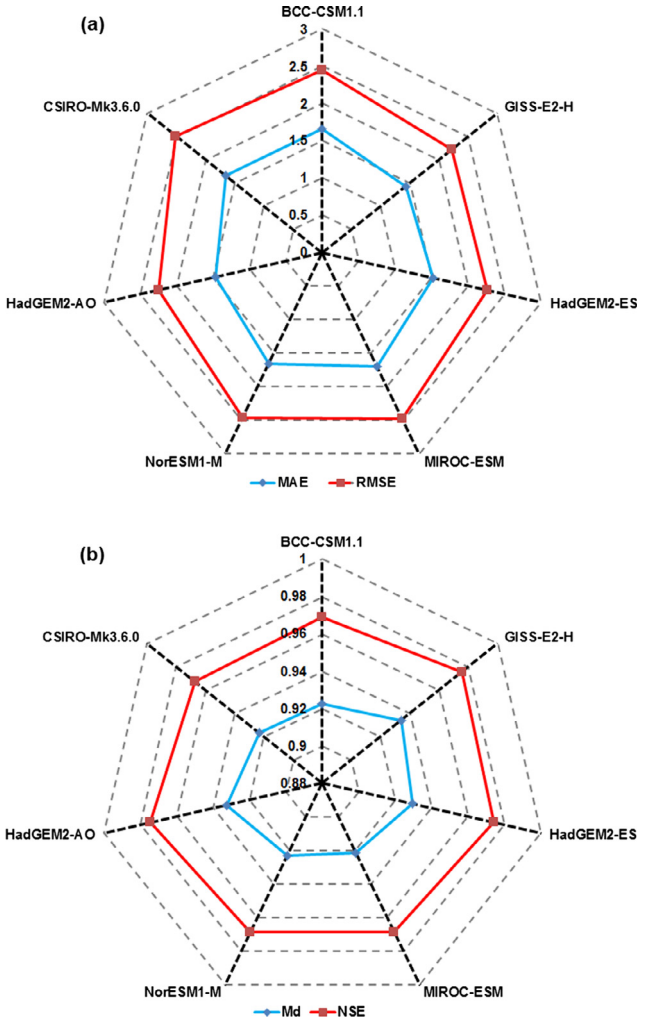

Fig. 4. (a) MAE and RMSE, and (b) Md and NSE of downscaled precipitation from support vector machine.

where F_o^{-1} is the quantile function corresponding to observed precipitation, and F_m is the cumulative distribution function of downscaled precipitation.

3.2.3. Performance evaluation

The performances of the GCMs were assessed using different statistics which are mean absolute error (MAE), root mean square error (RMSE), index of agreement (Md), and Nash–Sutcliffe model efficiency (NSE) to show the efficiency of models as follows:

$$MAE = \frac{1}{n}\sum_{i=1}^{n} |x_{obs,i} - x_{sim,i}| \tag{8}$$

$$RMSE = \left[\frac{1}{N}\sum_{i=1}^{N} (x_{sim,i} - x_{obs,i})^2\right]^{1/2} \tag{9}$$

$$md = 1 - \frac{\sum_{i=1}^{n} (x_{obs,i} - x_{sim,i})^j}{\sum_{i=1}^{n} (|x_{sim,i} - \bar{x_{obs}}| + |x_{obs,i} - \bar{x_{obs}}|)^j} \tag{10}$$

$$NSE = 1 - \frac{\sum_{i=1}^{N} (x_{sim,i} - x_{obs,i})^2}{\sum_{i=1}^{N} (x_{obs,i} - x_{obs})^2} \tag{11}$$

where, $x_{sim,i}$ and $x_{obs,i}$ are the i_{th} modeled and observed data, and N is the number of observations.

3.3. Drought analysis

3.3.1. Standardized precipitation Index (SPI)

SPI (McKee et al., 1993) provides a comparison of the precipitation over a specific period with the precipitation totals from the same period for all the recorded years and thus, facilitates the temporal analysis of droughts. In order to compute SPI, monthly precipitation data of each GPCC grid point were fitted with Normal, Lognormal, Gamma and Extreme Value-I distributions. The Kolmogorov-Smirnov (KS) test was conducted to estimate the goodness of fit to a particular distribution. The frequency distribution that best fit the data was used to compute the SPI value.

SPI gives positive and negative values where positive values define the wet conditions and negative values are used to classify the drought conditions. McKee et al. (1993) classified SPI values as mild drought ($SPI > -1.0$), moderate drought ($-1.5 < SPI \leq -1.0$), severe drought ($-2.0 < SPI \leq -1.5$) and extreme drought ($SPI \leq -2.0$).

SPI values were computed at the last month of a season defining the precipitation deficit of the entire season. For example, to measure droughts in late summer (August–October), a 3-month SPI in the month of October was used as it represents the precipitation deficit from August to October. A similar procedure was also adopted by Ahmed et al. (2015), Alamgir et al. (2015), and Mishra and Cherkauer (2010) for the calculation of seasonal droughts.

3.3.2. Development of SAF curves

A drought is usually considered a regional drought when the affected area reaches a threshold. The drought SAF curves are often used to represent all the characteristics of regional droughts (Henriques and Santos, 1999). The procedure adopted by several studies (Bonaccorso et al., 2015; Mishra and Desai, 2005; Mishra and Singh, 2009; Mishra and Cherkauer, 2010) was used in this study to develop SAF curves. After calculating SPI at each grid point, drought severities associated with different areal extents in the percentage of total area were calculated using ArcGIS.

For example, the 3-month SPI at the end of October was used to construct the SAF curves of late summer droughts. Therefore, the 3-month SPI at the end of October was associated with different areal extent in percentage of total area for different areal thresholds. In the present study, areal thresholds of 1, 2, 5, 10, 20, 30, 40, 50, 60, 70, 80, 90, and 100% were used. The probability distribution that best fits drought severity series for different areal extents were then determined. For this purpose, the drought severity for different areal extents were fitted with Normal, Lognormal, Gamma and Extreme Value-I distributions. Kolmogorov-Smirnov (KS) test was conducted to estimate the goodness of fit to a particular distribution. If the KS test statistics are found less than the critical table value, the null hypothesis of data following the specified distribution cannot be rejected. In this study, KS test statistics were found less than the critical table values for all areal extents when the drought severity series were compared with the gamma distribution. The p-values of KS test obtained during the fitting distribution of the Late Winter drought severity series for different areal extents are given in Table 2 as an example. A p-value higher than 0.05 indicates the KS test statistic is less than the critical values at $p = 0.05$ and therefore the null hypothesis cannot be rejected at 5% significance level. The table shows that the p-values were higher than 0.05 for all the cases when fitted with Gamma distribution. Similar results were also observed for other seasons. Therefore, Gamma distribution was selected and then its parameters were estimated using maximum goodness-of-fit estimation method. The gamma distribution parameters were used to estimate the return period of associated severity and areal extent. The return periods of 2, 5, 10, 25, 50 and 100 years were considered for analysis. The return period of associated severity and areal extent were finally plotted to prepare the SAF curves.

Table 2
The p-values of Kolmogorov-Smirnov test obtained during fitting distribution of the Late Winter drought severity series for different areal extents.

Area (%)	Distribution			
	Normal	Lognormal	Gamma	Extreme Value-I
1	0.000	0.008	0.471	0.041
2	0.000	0.160	0.369	0.831
5	0.001	0.219	0.117	0.935
10	0.014	0.547	0.958	0.463
20	0.039	0.413	0.899	0.599
30	0.385	0.893	0.975	0.638
40	0.412	0.988	0.798	0.737
50	0.393	0.928	0.707	0.890
60	0.882	0.983	0.883	0.805
70	0.215	0.299	0.355	0.489
80	0.718	0.683	0.669	0.142
90	0.930	0.950	0.960	0.180
100	0.939	0.882	0.848	0.870

3.3.3. *Uncertainty assessment in drought return periods*

Bayesian statistics was used to estimate the credible interval in the domain of the distribution of model output. In contrast to the frequentist confidence interval, Bayesian interval estimation considers related information from the prior distribution whereas confidence intervals are based only on the data rather than a large number of

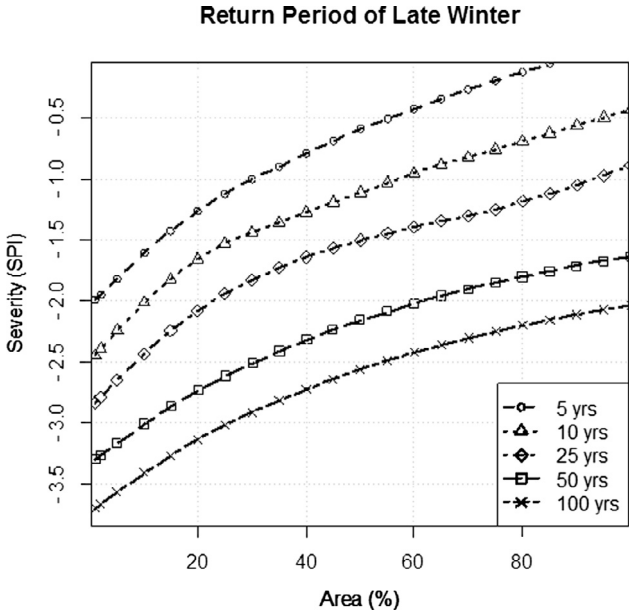

Fig. 6. SAF curves for Late Winter Season.

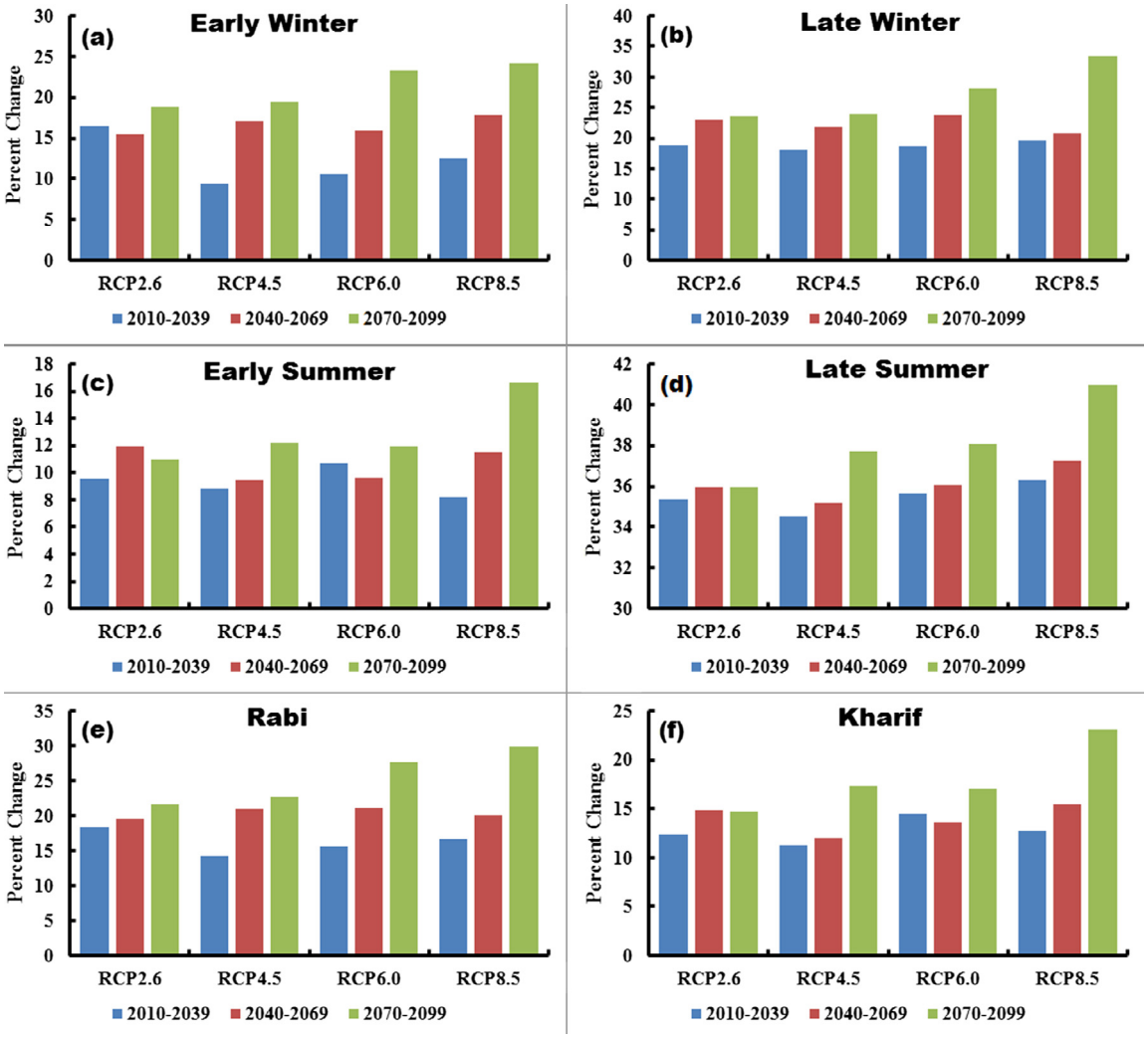

Fig. 5. Projected changes in ensemble precipitation obtained from (a) early winter; (b) late winter; (c) early summer; (d) late summer; (e) Rabi; and (f) Kharif seasons.

Table 3
Affected area (%) by historical droughts having return period of 5, 10, 25, 50, and 100 years.

Return Period	Severity	Late Winter	Early Winter	Early Summer	Late Summer	Rabi	Kharif
5	−1.00	30.36	38.48	33.23	32.84	30.23	33.47
	−1.50	13.06	11.49	12.82	10.49	10.10	10.30
	−2.00	0.00	0.00	0.00	0.00	0.00	0.00
	−2.50	0.00	0.00	0.00	0.00	0.00	0.00
	−3.00	0.00	0.00	0.00	0.00	0.00	0.00
10	−1.00	57.09	74.59	54.32	65.13	50.99	62.47
	−1.50	26.66	21.05	24.80	23.46	21.35	22.56
	−2.00	10.48	2.39	6.27	6.01	9.61	6.75
	−2.50	0.00	0.00	0.00	0.00	1.08	0.00
	−3.00	0.00	0.00	0.00	0.00	0.00	0.00
25	−1.00	93.40	100.00	83.71	100.00	87.87	100.00
	−1.50	50.34	41.44	44.41	49.90	63.76	47.69
	−2.00	22.80	9.40	15.20	15.84	28.49	20.06
	−2.50	8.46	0.00	1.85	2.67	11.22	3.98
	−3.00	0.00	0.00	0.00	0.00	1.52	0.00
50	−1.00	100.00	100.00	100.00	100.00	100.00	100.00
	−1.50	100.00	100.00	100.00	100.00	100.00	100.00
	−2.00	61.88	43.14	50.11	55.69	96.77	60.77
	−2.50	30.60	9.46	21.97	18.77	38.68	24.19
	−3.00	10.33	0.00	5.24	3.81	20.07	8.29
100	−1.00	100.00	100.00	100.00	100.00	100.00	100.00
	−1.50	100.00	100.00	100.00	100.00	100.00	100.00
	−2.00	100.00	100.00	100.00	100.00	100.00	98.38
	−2.50	54.23	26.72	42.63	43.41	72.53	51.17
	−3.00	25.76	6.88	18.16	15.20	35.17	24.26

repeated samples. For a given posterior, $P(M|R)$, the confidence interval for M $[M_{lo}, M_{hi}]$ is estimated using Bayesian approach as:

$$CI = \int_{M_{lo}}^{M_{hi}} P(M|R)dM \tag{12}$$

where CI is the confidence interval; M_{hi} and M_{lo} are the upper and lower bounds of confidence interval; M is model parameters; R is model output; the function $P(M)$ is the set of different probabilities for variable M; $\frac{P}{(M \mid R)dM}$ is the inverse probability distribution of R for given M; and dM represents normalization scale ($dM = 1$ indicates $P(M)$is normalized in a scale of 0–1. In this study, Bootstrap was applied on seven projected models to assess the return period at 2.5 and 97.5 quartiles (at 95% confidence interval) for a sample size of 1000. The 2.5 and 97.5 quartiles were defined as the lower and upper confidence levels. The detailed algorithm for BB can be found in Rubin (1981).

4. Results

4.1. Validation of CMIP5 models

The performances of downscaling models were numerically assessed by comparing the downscaled precipitation with GPCC precipitation for the period 1961–2005 using MAE, RMSE, Md, and NSE. Precipitation was downscaled at each GPCC grid point separately. The results obtained from area-averaged precipitation (average of 130 GPCC grid points) against downscaled area-averaged precipitation from GCMs are shown in Fig. 4. The MAE (Fig. 4a) values in all GCMs varied in the range of 1–2, while in RMSE values were found in the range of 2–2.5. The Md and NSE (Fig. 4b) values were also found high ranging from 0.92 to 0.98. GISS-E2-H was found the best GCM by showing lowest errors and highest agreement with observed data in term of all statistics.

4.2. Changes in annual seasonal ensemble precipitation

The projected changes in seasonal ensemble precipitation (2010–2039, 2040–2069, and 2070–2099) under RCP scenarios are shown in Fig. 5. It shows an increase in precipitation ranging from 8 to 41% in all seasons. RCP8.5 showed the maximum precipitation change especially during period 2070–2099. The differences among periods and scenarios were found small. A similar finding was also reported by Rashid et al. (2015) where differences among RCP scenarios were found small. Highest increase of about 41% was observed in late summer while the lowest (8%) in early summer.

4.3. SAF curves for historical droughts

The drought return periods of 5, 10, 25, 50, and 100 years were considered in the analysis. The SAF curves were plotted for climatic (SPI 3) and cropping seasons (SPI 6) on the basis of historical droughts (1961–2010). The SAF curve for late winter season is shown in Fig. 6 as an example.

Fig. 6 shows that drought with higher severity and higher return period cover a small portion of the study area. For example, a −3.0 (SPI) magnitude drought with a return period of 100 years covers an area of about 25.76% while the same magnitude drought with a return period of 50 years can affect an area of about 10.33%. On the other hand, droughts with lower return periods are less severe for the same areal extent than those of higher return periods. For example, a −1.0 (SPI) magnitude drought with a return period of 5 years can affect 30.36% of the area while the same magnitude drought with a return period of 10 years can affect 57.09% area.

The historical droughts with severities of −1, −1.5, −2.0, −2.5, and −3.0, for return periods of 5, 10, 25, 50, and 100 years were assessed to understand drought characteristics in different seasons. The affected areas by each category of droughts were estimated and presented in Table 3. The percentage of affected areas in different seasons and severity was found to vary. At lower return period and severity i.e. 5 years and −1 SPI, Early Winter drought was found to be the most affected that covers 38.48% while at high return period such as 100 years and −3 SPI, Rabi season was found to be the most affected season when drought can affect 35.17% of the total area. In addition, the percentage of the area was found to reduce from lower to higher severe droughts. For instance, in the late winter season at 25-year return period, a drought of −1.0 severity can affect 93.40% area and a drought of −1.5 severity can affect 50.34% area while 22.80, 8.46 and 0.0% are affected by drought at −2.0, −2.5 and −3 SPI respectively. Therefore, it can be remarked that on equal drought severity, larger areas are affected by drought as drought return period increases; on the other hand, on equal areal extent, drought severity increases as drought return period increases.

4.4. Uncertainties in projected droughts

The results obtained from BB at 95% confidence level of SAF curves were plotted to show the uncertainty in drought SAF for the future projected periods. Overall, 72 (6 seasons × 3 periods × 4 scenarios = 72) figures were prepared. The SAF curves for late winter season (2010–2039) under RCP2.6 are discussed and shown here as an example (Fig. 7). Each return period (5, 10, 25, 50, and 100 years) has three curves i.e. upper, middle, and lower. The upper curve represents the upper bound of 95% confidence interval of SAF curve, middle one represents the mean, and the lower curve represents the lower bounds. Narrower confidence band means the lower severity compared to droughts having a higher severity.

The area affected by drought with uncertainty bounds was investigated for all seasons and scenarios (6 seasons × 4 scenarios = 24 tables). The results obtained for late winter season under RCP2.6 scenario are shown in Table 4 as an example. A gradual increase in affected area can be seen between the bands (upper to lower). For example, a moderate drought of (SPI = −1) at 5-year return period can affect 23.6%, 30.7%, and 41.2% area for upper, middle and lower curve

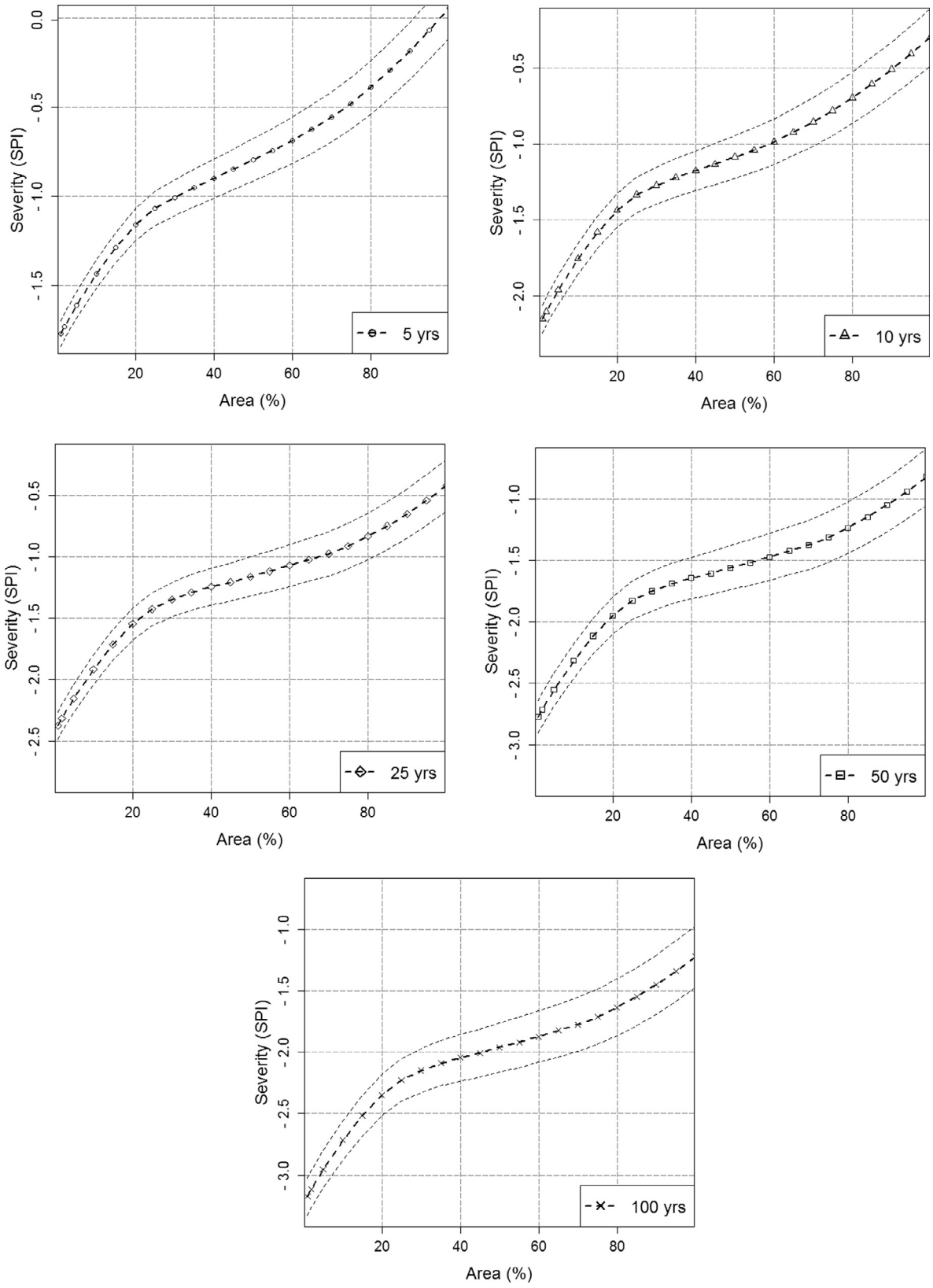

Fig. 7. SAF curves with confidence interval for Late Winter Season (2010 – 2039) under RCP2.6.

respectively. The differences were found small between the middle and lower bounds of droughts while a slightly higher difference was seen for the upper confidence bound of drought. Other seasons and scenarios also showed a similar kind of uncertainty. Similarly, a gradual increase in the affected area can be seen with return periods (low to high). For example, the area under the upper bound of drought starts increasing from 23.6% for 5-year return period to 98.8% for 100-year return period drought.

Table 4
Uncertainty in percent affected areas for late winter droughts obtained using Bayesian Bootstrap method.

Return Period/SPI Value		2010–2039					2040–2069					2070–2099				
		−1	−1.5	−2	−2.5	−3	−1	−1.5	−2	−2.5	−3	−1	−1.5	−2	−2.5	−3
5-Year	Upper	23.6	6.0	0.0	0.0	0.0	28.3	6.3	0.0	0.0	0.0	27.0	6.2	0.0	0.0	0.0
	Middle	30.7	8.2	0.0	0.0	0.0	36.3	8.9	0.0	0.0	0.0	34.5	8.7	0.0	0.0	0.0
	Lower	41.2	10.6	0.0	0.0	0.0	46.3	12.0	0.0	0.0	0.0	44.2	11.7	0.0	0.0	0.0
10-Year	Upper	44.7	14.3	2.2	0.0	0.0	47.5	15.6	0.0	0.0	0.0	45.9	15.2	0.0	0.0	0.0
	Middle	58.7	17.8	4.2	0.0	0.0	62.0	20.4	1.4	0.0	0.0	60.0	19.8	1.5	0.0	0.0
	Lower	71.0	22.3	6.4	0.0	0.0	76.0	27.2	4.4	0.0	0.0	73.9	26.0	4.5	0.0	0.0
25-Year	Upper	50.1	17.6	5.8	0.0	0.0	55.1	16.7	0.0	0.0	0.0	48.9	18.2	0.0	0.0	0.0
	Middle	67.4	22.0	8.2	0.0	0.0	73.1	23.7	2.2	0.0	0.0	68.4	24.3	3.8	0.0	0.0
	Lower	81.5	29.3	10.9	0.0	0.0	89.0	36.8	6.1	0.0	0.0	83.7	32.7	8.0	0.0	0.0
50-Year	Upper	81.3	37.4	14.3	3.5	0.0	87.8	44.1	11.6	0.0	0.0	83.3	38.9	13.3	NA	0.0
	Middle	92.3	57.0	18.4	6.1	0.0	100.0	62.1	18.0	0.0	0.0	95.5	56.6	19.4	0.0	0.0
	Lower	100.0	76.2	24.2	9.0	0.0	100.0	82.6	28.5	3.3	0.0	100.0	77.8	27.5	5.0	0.0
100-Year	Upper	98.8	74.0	28.1	11.4	1.4	100.0	79.3	34.0	7.1	0.0	100.0	75.4	31.2	8.8	0.0
	Middle	100.0	87.5	45.7	15.5	4.1	100.0	95.7	51.5	13.3	0.0	100.0	90.2	44.6	15.0	0.0
	Lower	100.0	98.7	69.4	20.7	7.3	100.0	100.0	75.5	21.9	0.0	100.0	100.0	70.5	22.9	2.2

Table 5
Percent changes in drought percent affected area (%) under RCP2.6.

Seasons	Return Period/ SPI Value	2010–2039					2040–2069					2070–2099				
		−1	−1.5	−2	−2.5	−3	−1	−1.5	−2	−2.5	−3	−1	−1.5	−2	−2.5	−3
Late Winter	5	0.38	−4.84	0.00	0.00	0.00	5.95	−4.15	0.00	0.00	0.00	4.12	−4.32	0.00	0.00	0.00
	10	1.56	−8.89	−6.31	0.00	0.00	4.95	−6.23	−9.06	0.00	0.00	2.91	−6.87	−8.93	0.00	0.00
	25	−26.00	−28.39	−14.57	−8.46	0.00	−20.31	−26.61	−20.60	−8.46	0.00	−25.05	−26.04	−18.95	−8.46	0.00
	50	−7.70	−43.01	−43.45	−24.48	−10.33	0.00	−37.91	−43.92	−30.60	−10.33	−4.51	−43.36	−42.49	−30.60	−10.33
	100	0.00	−12.54	−54.35	−38.77	−21.62	0.00	−4.29	−48.55	−40.89	−25.76	0.00	−9.81	−55.39	−39.21	−25.76
Early Winter	5	−6.66	−2.83	0.00	0.00	0.00	−2.90	−0.96	0.00	0.00	0.00	−3.97	−4.10	0.00	0.00	0.00
	10	−19.34	−1.86	−0.41	0.00	0.00	−15.99	1.86	1.35	0.00	0.00	−10.83	−2.70	−2.39	0.00	0.00
	25	−36.45	−18.64	−5.49	0.00	0.00	−32.41	−11.23	−1.99	0.00	0.00	−21.09	−20.15	−9.40	0.00	0.00
	50	−9.94	−45.25	−25.11	−8.43	0.00	−9.54	−39.66	−18.58	−5.65	0.00	0.00	−31.29	−27.35	−9.46	0.00
	100	0.00	−15.57	−54.65	−12.74	−6.88	0.00	−14.56	−48.35	−7.08	−6.88	0.00	0.00	−46.37	−15.50	−6.88
Early Summer	5	−1.59	−5.50	0.00	0.00	0.00	−1.86	−5.48	0.00	0.00	0.00	−0.01	−4.76	0.00	0.00	0.00
	10	0.76	−7.63	−4.57	0.00	0.00	4.46	−8.44	−6.27	0.00	0.00	1.92	−6.85	−3.49	0.00	0.00
	25	−20.48	−22.05	−12.40	−1.85	0.00	−14.94	−25.44	−13.87	−1.85	0.00	−18.27	−22.58	−2.28	5.01	1.97
	50	−4.57	−48.64	−32.42	−21.97	−5.24	−4.47	−43.05	−35.49	−21.97	−5.24	−9.63	−43.12	−30.81	−10.42	0.53
	100	0.00	−10.62	−58.18	−29.12	−18.16	0.00	−9.78	−56.88	−31.82	−18.16	0.00	−14.93	−53.13	−25.07	−7.98
Late Summer	5	1.76	−4.97	0.00	0.00	0.00	−0.49	−3.42	0.00	0.00	0.00	−4.67	−3.66	0.00	0.00	0.00
	10	1.57	−6.69	−6.01	0.00	0.00	−4.47	−6.27	−6.01	0.00	0.00	−13.60	−6.25	−6.01	0.00	0.00
	25	−16.58	−28.61	−15.84	−2.67	0.00	−30.00	−27.56	−13.86	−2.67	0.00	−41.65	−30.12	−15.84	−2.67	0.00
	50	0.00	−34.51	−39.66	−18.77	−3.81	0.00	−41.34	−38.50	−18.77	−3.81	−11.80	−50.97	−40.41	−18.77	−3.81
	100	0.00	0.00	−50.83	−31.92	−15.20	0.00	−5.04	−52.06	−30.60	−15.20	0.00	−18.60	−60.20	−32.20	−15.20
Rabi	5	4.20	−0.60	0.00	0.00	0.00	4.31	−1.43	0.00	0.00	0.00	5.80	−1.26	0.00	0.00	0.00
	10	4.62	−1.23	−6.23	−1.08	0.00	14.24	−3.61	−9.61	−1.08	0.00	13.85	0.25	−8.35	−1.08	0.00
	25	−24.38	−39.20	−22.74	−11.22	−1.52	−14.09	−42.99	−28.49	−11.22	−1.52	−15.26	−36.80	−24.83	−11.22	−1.52
	50	−4.50	−46.28	−76.95	−35.83	−20.07	0.00	−36.96	−81.21	−38.68	−20.07	0.00	−38.26	−76.00	−38.68	−20.07
	100	0.00	−10.82	−55.01	−56.66	−35.17	0.00	−0.45	−49.43	−61.40	−35.17	0.00	0.00	−48.32	−56.72	−35.17
Kharif	5	2.85	−1.39	0.00	0.00	0.00	0.86	−2.22	0.00	0.00	0.00	−2.63	−3.32	0.00	0.00	0.00
	10	−0.81	−3.22	−6.75	0.00	0.00	−2.72	−2.10	−6.75	0.00	0.00	−7.28	−5.60	−6.75	0.00	0.00
	25	−29.48	−23.03	−14.88	−3.98	0.00	−28.62	−23.05	−17.31	−3.98	0.00	−39.51	−27.92	−20.06	−3.98	0.00
	50	−4.95	−36.90	−41.44	−21.74	−8.29	0.00	−41.51	−41.31	−24.19	−8.29	−9.91	−50.64	−45.51	−24.19	−8.29
	100	0.00	−10.53	−43.67	−36.03	−24.26	0.00	−4.51	−51.88	−36.38	−24.26	0.00	−15.81	−58.78	−39.96	−24.26

4.5. Percent changes in drought area

The SAF curves were further analyzed to assess the changes in drought characteristics due to climate change. The assessments were carried out by comparing the SAF curves with uncertainty under projected climate with the SAF curves prepared with historical GPCC precipitation. The comparison was made for all scenarios and for all seasons. The obtained results for mean SAF curves under RCP2.6, RCP4.5, RCP6.0, and RCP8.5 scenarios are provided in Tables 5–8, respectively as examples. The tables show the results for three different periods (2010–2039, 2040–2069, and 2070–2099), six seasons (early winter, late winter, early summer, later summer, Rabi, and Kharif), five return periods (5, 10, 25, 50, and 100 years), and five drought severities (−1, −1.5, −2.0, −2.5, and −3.0). The negative values represent reduced the affected area and the positive values represent more affected area by future droughts.

Table 5 for RCP2.6 shows that the percentage of area affected by droughts varies from season to season, and for different drought

Table 6
Percent changes in drought percent affected area (%) under RCP4.5.

Seasons	Return Period/ SPI Value	2010–2039					2040–2069					2070–2099				
		−1	−1.5	−2	−2.5	−3	−1	−1.5	−2	−2.5	−3	−1	−1.5	−2	−2.5	−3
Late Winter	5	1.29	−5.05	0.00	0.00	0.00	−0.68	−5.82	0.00	0.00	0.00	2.84	−4.31	0.00	0.00	0.00
	10	−1.36	−9.01	−9.09	0.00	0.00	−1.45	−10.37	−10.48	0.00	0.00	0.57	−7.55	−7.56	0.00	0.00
	25	−31.62	−29.08	−18.29	−8.46	0.00	−29.77	−30.66	−20.17	−8.46	0.00	−26.82	−27.88	−17.96	−8.46	0.00
	50	−5.24	−51.29	−44.57	−28.79	−10.33	−8.25	−49.23	−46.28	−30.60	−10.33	−11.21	−42.93	−43.94	−28.36	−10.33
	100	0.00	−12.05	−61.26	−40.50	−25.76	0.00	−13.47	−60.36	−42.26	−25.76	0.00	−15.53	−54.69	−40.07	−25.76
Early Winter	5	−10.63	−4.03	0.00	0.00	0.00	−6.66	−2.83	0.00	0.00	0.00	−5.49	−1.77	0.00	0.00	0.00
	10	−25.22	−5.34	−2.39	0.00	0.00	−17.71	−2.46	0.38	0.00	0.00	−12.65	−1.29	1.03	0.00	0.00
	25	−41.69	−22.96	−6.98	0.00	0.00	−35.40	−19.84	−5.36	0.00	0.00	−27.62	−17.27	−3.90	0.00	0.00
	50	−8.19	−53.57	−28.52	−9.46	0.00	−6.20	−44.63	−25.97	−8.06	0.00	0.00	−42.52	−23.63	−6.87	0.00
	100	0.00	−15.46	−63.38	−15.51	−6.88	0.00	−12.72	−54.90	−13.33	−6.88	0.00	−6.16	−55.50	−11.17	−6.88
Early Summer	5	−3.91	−6.00	0.00	0.00	0.00	−1.43	−5.49	0.00	0.00	0.00	−0.06	−4.71	0.00	0.00	0.00
	10	−2.67	−7.88	−5.06	0.00	0.00	1.27	−7.10	−5.25	0.00	0.00	4.53	−7.13	−6.27	0.00	0.00
	25	−26.64	−23.36	−10.33	−1.85	0.00	−18.84	−23.00	−12.59	−1.85	0.00	−16.27	−23.11	−11.66	−1.85	0.00
	50	−10.27	−52.43	−32.90	−19.65	−5.24	−5.18	−44.90	−33.27	−21.97	−5.24	−4.74	−41.71	−33.22	−21.97	−5.24
	100	0.00	−16.88	−61.07	−28.88	−18.16	0.00	−11.68	−55.67	−29.82	−18.16	0.00	−10.81	−52.36	−29.57	−18.16
Late Summer	5	−1.89	−4.93	0.00	0.00	0.00	−3.46	−4.38	0.00	0.00	0.00	−1.66	−1.27	0.00	0.00	0.00
	10	−4.53	−6.83	−6.01	0.00	0.00	−12.06	−6.84	−6.01	0.00	0.00	−9.94	−5.82	−2.14	0.00	0.00
	25	−27.25	−30.66	−12.89	−2.67	0.00	−38.18	−30.09	−13.30	−2.67	0.00	−38.88	−28.74	−8.04	−2.67	0.00
	50	0.00	−47.08	−40.42	−18.77	−3.81	−9.55	−50.43	−39.99	−18.77	−3.81	−5.01	−49.79	−37.84	−13.08	−3.81
	100	0.00	0.00	−59.75	−31.60	−15.20	0.00	−15.04	−60.50	−31.39	−15.20	0.00	−11.82	−59.16	−28.51	−11.45
Rabi	5	2.94	−1.97	0.00	0.00	0.00	5.55	−1.17	0.00	0.00	0.00	5.55	−1.17	0.00	0.00	0.00
	10	7.66	−3.98	−9.61	−1.08	0.00	9.36	−0.88	−9.61	−1.08	0.00	9.36	−0.88	−9.61	−1.08	0.00
	25	−22.79	−42.96	−25.24	−11.22	−1.52	−22.39	−38.47	−24.74	−11.22	−1.52	−22.39	−38.47	−24.74	−11.22	−1.52
	50	−4.37	−46.67	−80.26	−38.68	−20.07	0.00	−43.58	−76.89	−38.68	−20.07	0.00	−43.58	−76.89	−38.68	−20.07
	100	0.00	−10.05	−57.13	−59.80	−35.17	0.00	−6.68	−52.32	−57.22	−35.17	0.00	−6.68	−52.32	−57.22	−35.17
Kharif	5	0.86	−2.22	0.00	0.00	0.00	1.31	−2.96	0.00	0.00	0.00	1.10	−2.97	0.00	0.00	0.00
	10	−0.65	−4.12	−3.94	0.00	0.00	−2.57	−4.17	−6.75	0.00	0.00	0.29	−3.57	−6.75	0.00	0.00
	25	−29.67	−24.83	−13.22	−3.98	0.00	−31.78	−25.57	−20.06	−3.98	0.00	−28.45	−25.20	−17.71	−3.98	0.00
	50	0.00	−43.16	−42.16	−19.78	−8.29	−4.78	−41.35	−44.34	−24.19	−8.29	−4.62	−38.25	−43.41	−24.19	−8.29
	100	0.00	−7.78	−51.91	−36.02	−22.05	0.00	−10.45	−50.23	−39.67	−24.26	0.00	−9.50	−49.83	−38.14	−24.26

severities. Most of the cases droughts were found to be reduced while some increases were found in almost all seasons at 5 and 10-year return periods. Rabi season was found to be the most affected at 10-years return period by moderate drought (−1.0 SPI) during 2040–2069. The 5-year return period droughts (−1 SPI) in this season were also found to increase (5.80%) during 2070–2099.

In Table 6 for RCP4.5, higher negative values can be seen indicating fewer droughts covering less area. On the other hand, small positive values can be found for lower severities indicating more droughts covering small area. The percentages of areas affected by droughts were found to vary from season to season. However, most of the seasons were found to show negative values for drought severities of −2.0 and above, and positive values for drought severities of −1.0 and below. Early winter was the only season that does not show any increase in drought. Rabi season was found to show the highest drought increase (9.36%) at −1 SPI during 2040–2069. The same was also noticed under RCP2.6 where Rabi season showed the highest increase at 10-year return period.

In Table 7 for RCP6.0, it can be noted that results are similar to those of RCP2.6 and RCP4.5 scenarios. However, a few differences can be seen in Table 7. Similar to RCP2.6 and RCP4.5, Rabi seasons showed the highest increase in drought affected area under RCP6.0, except 50-year return period at −2 SPI during 2070–2099 when Rabi drought is found to decrease up to −78.74%. Overall, drought was found to be more at low severity (-1 SPI) and return period (5-years) and vice versa. For example, at −1 SPI and at 5-year return period drought was projected to increase while decrease at −3 SPI and at 100-year return period over the present century.

Under RCP8.5 scenario (Table 8), moderate droughts (-1 SPI) for the 5-year return period will continuously increase in Rabi, Kharif and late winter seasons. These droughts will affect more areas during 2040–2069 where Rabi and Kharif seasons will be the most affected with the increase by 7.78% and 6.2%, respectively. It was noticed that droughts in most cases will reduce while in few cases it will increase. This increase will be more in the Rabi season (14.02%, moderate droughts for 10-year return period) which is also found under RCP2.6, RCP4.5 and RCP8.5 scenarios. It was also noticed that most of the zeros (or no change) were for −2 and above SPI (extreme droughts) at 5-year return period.

5. Discussions

Balochistan is predominantly characterized by an arid climate. Precipitation is the major source of water for agriculture that is critically important for the livelihoods of the majority of the population in the province. Thus, it is very important to understand future changes and variability in precipitation on the eve of climate change. This study projected the future precipitation of Balochistan, Pakistan from seven CMIP5 GCMs for four RCP scenarios using SVM.

Several studies (Wilby and Wigley, 1997; Wilby et al., 1998) have been conducted to determine the best downscaling method and reported that different downscaling methods generate radically different future projections for the same GCM predictors. In order to avoid different future projections from the same GCM model, this study used SVM downscaling technique. The performance of SVM downscaling model was rigorously tested using various robust statistical tests. The result obtained from different statistics reflects the high capability of SVM in downscaling precipitation at arid region.

Future changes in precipitation of GCMs are often expected to yield a greater increase in precipitation under RCP8.5 compared to those in other RCPs especially for the 2070s (Ouyang et al., 2015; Villarini et al., 2015; Yin et al., 2015). Similar results were obtained in the present

Table 7
Percent changes in drought percent affected area (%) under RCP6.0.

Seasons	Return Period/ SPI Value	2010–2039					2040–2069					2070–2099				
		−1	−1.5	−2	−2.5	−3	−1	−1.5	−2	−2.5	−3	−1	−1.5	−2	−2.5	−3
Late Winter	5	2.87	−4.94	0.00	0.00	0.00	1.46	−4.40	0.00	0.00	0.00	1.31	−5.22	0.00	0.00	0.00
	10	1.80	−6.65	−7.23	0.00	0.00	−2.29	−8.19	−8.97	0.00	0.00	−0.23	−8.23	−10.48	0.00	0.00
	25	−28.73	−25.12	−20.14	−8.46	0.00	−33.09	−29.50	−18.72	−8.46	0.00	−30.49	−29.93	−17.83	−8.46	0.00
	50	−9.61	−44.18	−42.03	−30.60	−10.33	−12.68	−48.37	−45.16	−29.07	−10.33	−6.13	−47.81	−45.22	−27.92	−10.33
	100	0.00	−14.95	−53.80	−39.16	−25.76	0.00	−18.05	−57.06	−41.12	−25.76	0.00	−12.59	−57.59	−40.90	−25.76
Early Winter	5	−7.26	−2.79	0.00	0.00	0.00	−9.16	−4.66	0.00	0.00	0.00	−5.39	−1.74	0.00	0.00	0.00
	10	−18.43	−2.06	−0.09	0.00	0.00	−23.56	−4.73	−0.80	0.00	0.00	−14.50	−0.24	0.72	0.00	0.00
	25	−33.62	−17.74	−3.59	0.00	0.00	−41.79	−22.74	−6.19	0.00	0.00	−28.54	−15.28	−4.80	0.00	0.00
	50	−7.67	−41.18	−24.11	−6.31	0.00	−12.84	−52.20	−28.20	−9.46	0.00	−7.26	−38.30	−22.61	−8.08	0.00
	100	0.00	−13.78	−50.63	−11.55	−6.88	0.00	−18.37	−63.23	−15.03	−6.88	0.00	−11.54	−49.49	−10.75	−6.88
Early Summer	5	1.53	−6.21	0.00	0.00	0.00	3.06	−4.56	0.00	0.00	0.00	0.08	−3.51	0.00	0.00	0.00
	10	2.48	−6.76	−6.27	0.00	0.00	6.45	−4.02	−6.27	0.00	0.00	0.77	−4.58	−4.04	0.00	0.00
	25	−17.11	−22.31	−13.90	−1.85	0.00	−10.89	−20.13	−10.90	−1.85	0.00	−20.48	−18.22	−10.59	−1.85	0.00
	50	−5.30	−41.54	−33.38	−21.97	−5.24	0.00	−38.04	−31.18	−20.54	−5.24	−10.01	−44.78	−29.39	−20.66	−5.24
	100	0.00	−11.80	−50.43	−30.39	−18.16	0.00	−0.03	−48.65	−28.00	−18.16	0.00	−15.78	−52.82	−26.47	−18.16
Late Summer	5	−1.88	−2.45	0.00	0.00	0.00	−1.24	−2.49	0.00	0.00	0.00	3.37	−1.05	0.00	0.00	0.00
	10	−2.27	−7.17	−6.01	0.00	0.00	−7.77	−4.88	−4.88	0.00	0.00	−0.95	−1.51	−2.99	0.00	0.00
	25	−24.06	−29.24	−11.53	−2.67	0.00	−34.97	−26.96	−11.47	−2.67	0.00	−24.26	−21.51	−8.53	−2.67	0.00
	50	0.00	−42.04	−38.97	−17.00	−3.81	−4.92	−47.19	−37.26	−17.32	−3.81	0.00	−37.17	−33.12	−14.52	−3.81
	100	0.00	0.00	−57.77	−30.21	−15.20	0.00	−10.76	−57.70	−28.96	−15.20	0.00	0.00	−48.17	−25.39	−13.76
Rabi	5	6.11	−2.57	0.00	0.00	0.00	4.37	−1.76	0.00	0.00	0.00	4.26	−2.00	0.00	0.00	0.00
	10	8.93	−0.94	−9.61	−1.08	0.00	5.47	−1.17	−7.17	−1.08	0.00	7.62	−2.57	−8.21	−1.08	0.00
	25	−17.72	−39.48	−26.38	−11.22	−1.52	−24.97	−40.43	−21.28	−11.22	−1.52	−22.35	−40.66	−25.09	−11.22	−1.52
	50	−7.43	−39.65	−78.39	−38.68	−20.07	−12.25	−44.77	−77.94	−33.86	−20.07	0.00	−43.41	−78.74	−38.68	−20.07
	100	0.00	−11.96	−49.33	−58.90	−35.17	0.00	−17.38	−52.39	−57.13	−32.45	0.00	−6.68	−51.94	−58.74	−35.17
Kharif	5	2.66	−2.06	0.00	0.00	0.00	3.37	−0.54	0.00	0.00	0.00	2.06	−0.31	0.00	0.00	0.00
	10	4.02	−2.11	−6.75	0.00	0.00	1.97	0.96	−3.78	0.00	0.00	−1.99	−0.55	−2.97	0.00	0.00
	25	−21.98	−20.99	−16.37	−3.98	0.00	−24.69	−15.43	−14.45	−3.98	0.00	−30.34	−18.38	−11.35	−3.98	0.00
	50	0.00	−32.38	−40.28	−24.19	−8.29	0.00	−35.74	−36.26	−22.20	−8.29	−4.39	−40.00	−36.72	−18.65	−8.29
	100	0.00	0.00	−43.07	−35.58	−24.26	0.00	0.00	−44.07	−32.45	−24.26	0.00	−9.93	−48.54	−31.61	−21.69

study. The higher increase in precipitation was observed in southeast parts of Balochistan during monsoon, which indicates that the monsoon will be more intense in future. Menon et al. (2013) also noticed a consistent increase in monsoon precipitation.

Historical SAF curves clearly showed that, on equal drought severity, drought areal extent increases as drought return period increases. It was observed that a drought with a severity of −1.0 can affect more than 30% area in all seasons at 5-year return period, while the whole study area (100%) can be affected if the drought return period increases to 50 years. The results also revealed that the affected area of droughts varies from season to season; however, early winter season was the most affected season.

The projected SAF curves for all seasons indicated that drought with higher severity and high return periods cover a small portion of the study area. Similar results were also shown in other studies (Akhtari et al., 2008; Mishra and Singh, 2009; Mishra and Cherkauer, 2010). They reported that droughts with higher return period and severity can influence less area and droughts with lower return periods can cover more area.

The projected results indicate that there will be more droughts in future with low severity and return periods. Overall, high reduction in drought was observed in all scenarios and periods (2010–2039, 2040–2069, and 2070–2099) and a small increase for few cases. Overall, the change in affected area would vary from −81.21% to 14.2%.

Reflection of GCM uncertainties in estimated drought return period cannot be ruled out (Lee and Kim, 2013). BB used in this study provided a range of values that are helpful to understand the changes that may occur in future drought. The range of uncertainty provided basic information for taking proper adaptation measures.

Increased risk of droughts has been projected in many regions due to the increased variability of precipitation (Taylor et al., 2013). Temporal analysis of projected precipitation in this study showed an increase in precipitation; however, the increased precipitation doesn't confirm the reduction of droughts for all severities and return periods. The droughts were found more severe with low return periods covering larger areas. The similar was also reported in IPCC (2007) where they reported higher intensity and longer duration droughts over larger areas. Kundzewicz et al. (2008) reported that the regions that often experienced drought are highly prone to projected droughts. It indicates that areal extents of droughts will increase due to climate change. This is partially true for the present study area where drought area was found to increase in some seasons i.e. early winter, Rabi and Kharif.

6. Conclusions

This study employed SPI to characterize seasonal droughts by developing SAF curves over Balochistan, Pakistan. Seven CMIP5 GCMs precipitation were downscaled using SVM method for historical period in order to assess the capability of the downscaling model in reproducing historical precipitation and subsequently used for future projection of precipitation. The SAF curves were developed based on GPCC historical and downscaled CMIP5 GCM precipitation. BB was used to estimate the uncertainty in future droughts. Additionally, the historical and projected SAF curves were compared to understand the changes in future droughts.

The main findings of the study are: (1) SVM model was successfully validated in downscaling CMIP5 GCMs precipitation. (2) All climate models revealed the increased precipitation especially in the last part of the century (2070–2099) under all RCP scenarios. This increase in precipitation will be gradual over the period from 2010 to 2099. Overall, precipitation was projected to increase in different seasons in

Table 8
Percent changes in drought percent affected area (%) under RCP8.5.

Seasons	Return Period/ SPI Value	2010–2039					2040–2069					2070–2099				
		−1	−1.5	−2	−2.5	−3	−1	−1.5	−2	−2.5	−3	−1	−1.5	−2	−2.5	−3
Late Winter	5	0.76	−4.94	0.00	0.00	0.00	2.92	−4.99	0.00	0.00	0.00	2.81	−3.77	0.00	0.00	0.00
	10	−2.32	−8.26	−8.74	0.00	0.00	−1.05	−8.54	−7.91	0.00	0.00	0.12	−6.67	−7.09	0.00	0.00
	25	−30.04	−28.51	−17.23	−8.46	0.00	−29.45	−30.57	−18.77	−8.46	0.00	−28.22	−24.73	−16.05	−8.46	0.00
	50	−9.86	−46.78	−44.07	−27.53	−10.33	−8.29	−47.07	−45.89	−29.02	−10.33	−11.63	−42.80	−41.90	−26.51	−10.33
	100	0.00	−15.40	−57.45	−39.93	−25.76	0.00	−13.60	−58.55	−41.61	−25.76	0.00	−16.30	−50.69	−38.05	−24.10
Early Winter	5	−7.99	−3.34	0.00	0.00	0.00	−6.71	−2.30	0.00	0.00	0.00	−5.55	−0.81	0.00	0.00	0.00
	10	−21.01	−3.15	−0.90	0.00	0.00	−19.96	−1.54	0.26	0.00	0.00	−17.75	1.36	3.31	0.00	0.00
	25	−40.25	−20.57	−5.51	0.00	0.00	−36.26	−18.36	−2.93	0.00	0.00	−33.79	−13.44	−0.58	0.00	0.00
	50	−5.06	−50.05	−26.37	−8.22	0.00	−11.89	−45.20	−24.38	−5.52	0.00	−5.28	−41.90	−20.32	−3.44	0.00
	100	0.00	−12.52	−58.95	−13.58	−6.88	0.00	−16.71	−54.74	−11.54	−5.29	0.00	−11.85	−50.31	−8.07	−3.49
Early Summer	5	−2.41	−5.81	0.00	0.00	0.00	3.33	−5.45	0.00	0.00	0.00	1.14	−3.56	0.00	0.00	0.00
	10	1.18	−7.43	−6.27	0.00	0.00	11.05	−4.30	−6.27	0.00	0.00	5.68	−4.98	−3.73	0.00	0.00
	25	−19.84	−23.62	−8.65	−1.85	0.00	−5.07	−19.64	−12.79	−1.85	0.00	−12.15	−20.22	−9.72	−1.85	0.00
	50	−4.54	−46.94	−32.84	−17.64	−5.24	0.00	−31.88	−31.32	−21.97	−5.24	−4.62	−38.25	−30.68	−19.35	−5.24
	100	0.00	−10.73	−56.99	−28.48	−15.84	0.00	0.00	−44.27	−28.66	−18.16	0.00	−9.50	−52.07	−27.19	−18.16
Late Summer	5	−3.16	−3.49	0.00	0.00	0.00	−3.25	−2.84	0.00	0.00	0.00	−1.01	−1.88	0.00	0.00	0.00
	10	−7.63	−6.10	−3.95	0.00	0.00	−9.09	−6.90	−3.06	0.00	0.00	−9.76	−4.89	−3.08	0.00	0.00
	25	−32.40	−28.98	−9.93	−2.67	0.00	−34.77	−29.59	−10.28	−2.67	0.00	−37.78	−27.67	−12.10	−2.67	0.00
	50	−7.32	−45.10	−38.48	−15.14	−3.81	−6.14	−50.13	−38.82	−15.56	−3.81	−6.30	−47.42	−37.93	−18.77	−3.81
	100	0.00	−11.89	−57.03	−29.46	−13.72	0.00	−12.02	−62.75	−29.73	−15.20	0.00	−13.49	−57.19	−29.62	−15.20
Rabi	5	4.53	−2.05	0.00	0.00	0.00	7.78	−1.80	0.00	0.00	0.00	2.84	−0.84	0.00	0.00	0.00
	10	9.36	−2.64	−9.61	−1.08	0.00	14.02	−2.82	−9.61	−1.08	0.00	5.74	−1.42	−8.12	−1.08	0.00
	25	−18.30	−41.66	−27.31	−11.22	−1.52	−12.91	−41.46	−26.20	−11.22	−1.52	−26.28	−40.19	−22.78	−11.22	−1.52
	50	−4.58	−40.79	−79.96	−38.68	−20.07	0.00	−34.33	−79.82	−38.68	−20.07	−4.40	−48.28	−77.72	−35.71	−20.07
	100	0.00	−9.83	−51.94	−60.22	−35.17	0.00	−4.64	−44.94	−59.91	−35.17	0.00	−10.97	−56.68	−57.28	−35.17
Kharif	5	2.82	−1.39	0.00	0.00	0.00	6.20	−2.09	0.00	0.00	0.00	3.50	−0.51	0.00	0.00	0.00
	10	−2.07	−1.93	−6.75	0.00	0.00	8.91	−0.46	−4.46	0.00	0.00	−0.03	−0.57	−4.75	0.00	0.00
	25	−32.27	−23.73	−17.12	−3.98	0.00	−15.71	−19.97	−13.31	−3.98	0.00	−30.58	−16.72	−14.45	−3.98	0.00
	50	0.00	−41.08	−42.17	−24.19	−8.29	0.00	−26.58	−39.78	−20.18	−8.29	0.00	−40.16	−37.02	−22.11	−8.29
	100	0.00	−6.76	−48.86	−37.08	−24.26	0.00	0.00	−36.49	−34.53	−22.74	0.00	−5.98	−46.78	−32.89	−24.26

the range of 8% to 41% over the region by the end of this century. (3) The historical SAF curves revealed that the higher return period e.g., 25-, 50-, 100-years, but less severe (SPI < -2.0) droughts are more in the study area. The drought-affected areas vary from season to season. Droughts during Rabi season affect larger area as compared with other seasons. (4) Changes in future drought area revealed that the droughts with low severities (SPI $= -1.0$) and return periods (≤ 10 years) will increase in most of the seasons. On the other hand, affected area by droughts with high severity (SPI ≥ -1.5) and return periods (≥ 25 years) will be reduced under all climate change scenarios. However, no consistency in the reduction of less severe droughts was found for different climate change scenarios. (5) The uncertainty band of drought SAF curves estimated using BB at a 95% confidence level revealed that uncertainty ranges were different for different return periods and seasons. Overall, the SAF curves with higher return periods are found to be more uncertain compared to those for lower return periods. Therefore, it can be concluded that the projection of increased extreme droughts in the study area is highly uncertain.

In the present study, possible changes in drought characteristics due to climate change are assessed using seven GCMs and SPI. However, more GCMs and other drought indices can be used to have greater insight into future drought characteristics in the study area. It is expected that the SAF curves generated in this study will assist in disaster risk management and mitigation planning.

Acknowledgments

This work is supported by the Post-Doctoral Fellowship Scheme of Universiti Teknologi Malaysia (PDRU) Grant No. Q.J130000.21A2.04E10. We acknowledge the World Climate Research Programme's working Group on coupled Modelling, which is responsible for CMIP, and we thank the modelling groups for producing and making available their model output. We are also thankful to the developers of GPCC, for providing gridded precipitation datasets.

Appendix A. Supplementary data

Supplementary data to this article can be found online at https://doi.org/10.1016/j.jhydrol.2019.01.019.

References

Acton, Q.A., 2012. Advances in Machine Learning Research and Application: 2012 Edition. Scholarly Editions.
Ahmed, K., Shahid, S., Harun, S.B., Wang, X.-J., 2015. Characterization of seasonal droughts in Balochistan Province, Pakistan. Stochastic Environ. Res. Risk Assess. 30 (2), 747–762. https://doi.org/10.1007/s00477-015-1117-2.
Akhtari, R., Bandarabadi, S., Saghafian, B., 2008. Spatio-temporal pattern of drought in Northeast of Iran. International Conference on Drought management: Scientific and Technological Innovations. Citeseer.
Alamgir, M., Shahid, S., Hazarika, M.K., Nashrrullah, S., Harun, S.B., Shamsudin, S., 2015. Analysis of meteorological drought pattern during different climatic and cropping seasons in Bangladesh. JAWRA J. Am. Water Resour. Assoc. 51 (3), 794–806.
Anjum, S., Saleem, M., Cheema, M., Bilal, M., Khaliq, T., 2012. An assessment to vulnerability, extent, characteristics and severity of drought hazard in Pakistan. Pak. J. Sci. 64 (2).
Asefa, T., Kemblowski, M.W., Urroz, G., McKee, M., Khalil, A., 2004. Support vectors–based groundwater head observation networks design. Water Resour. Res. 40 (11).
Ashraf, M., Routray, J.K., 2015. Spatio-temporal characteristics of precipitation and drought in Balochistan Province, Pakistan. Nat. Hazards 77 (1), 229–254.
Ashraf, M., Routray, J.K., Saeed, M., 2014. Determinants of farmers' choice of coping and adaptation measures to the drought hazard in northwest Balochistan, Pakistan. Nat. Hazards 73 (3), 1451–1473. https://doi.org/10.1007/s11069-014-1149-9.
Becker, A., Finger, P., Meyer-Christoffer, A., Rudolf, B., Schamm, K., Schneider, U., Ziese, M., 2013. A description of the global land-surface precipitation data products of the Global Precipitation Climatology Centre with sample applications including centennial (trend) analysis from 1901–present. Earth Syst. Sci. Data 5 (1), 71–99.

https://doi.org/10.5194/essd-5-71-2013.
Bonaccorso, B., Peres, D.J., Castano, A., Cancelliere, A., 2015. SPI-based probabilistic analysis of drought areal extent in sicily. Water Resour. Manage. 29 (2), 459–470. https://doi.org/10.1007/s11269-014-0673-4.
Burke, E.J., Brown, S.J., 2008. Evaluating uncertainties in the projection of future drought. J. Hydrometeorol. 9 (2), 292–299.
Burke, E.J., Brown, S.J., 2010. Regional drought over the UK and changes in the future. J. Hydrol. 394 (3–4), 471–485. https://doi.org/10.1016/j.jhydrol.2010.10.003.
Chen, H., Sun, J., Chen, X., 2014. Projection and uncertainty analysis of global precipitation-related extremes using CMIP5 models. Int. J. Climatol. 34 (8), 2730–2748.
Dai, A., Zhao, T., 2016. Uncertainties in historical changes and future projections of drought. Part I: estimates of historical drought changes. Clim. Change 144 (3), 519–533. https://doi.org/10.1007/s10584-016-1705-2.
Dibike, Y.B., Velickov, S., Solomatine, D., Abbott, M.B., 2001. Model induction with support vector machines: introduction and applications. J. Comput. Civ. Eng.
Eden, J.M., Widmann, M., Grawe, D., Rast, S., 2012. Skill, correction, and downscaling of GCM-simulated precipitation. J. Clim. 25 (11), 3970–3984. https://doi.org/10.1175/jcli-d-11-00254.1.
Efron, B., 1992. Bootstrap Methods: Another Look at the Jackknife. Springer.
Forouzani, M., Karami, E., 2010. Agricultural water poverty index and sustainability. Agron. Sustainable Dev.
GoB, 2014. Balochistan, Pakistan. http:// www.balochistan.gov.pk/index.php?option=com_content& view=article&id=37&Itemid=783 (Accessed 15 June 2016).
Gudmundsson, L., Bremnes, J., Haugen, J., Engen-Skaugen, T., 2012. Technical note: downscaling RCM precipitation to the station scale using statistical transformations–a comparison of methods. Hydrol. Earth Syst. Sci. 16 (9), 3383–3390.
Henriques, A., Santos, M., 1999. Regional drought distribution model. Phys. Chem. Earth Part B 24 (1), 19–22.
Hu, Y.-M., Liang, Z.-M., Liu, Y.-W., Zeng, X.-F., Wang, D., 2015. Uncertainty assessment of estimation of hydrological design values. Stochastic Environ. Res. Risk Assess. 29 (2), 501–511.
Hussein, M.H., 2004. Bonded Labour in Agriculture: A Rapid Assessment in Sindh and Balochistan, Pakistan. International Labour Organization.
IPCC, 2007. Climate Change 2007-The Physical Science Basis: Working Group I Contribution to the Fourth Assessment Report of the IPCC, 4. Cambridge University Press.
Kazmi, D.H., Li, J., Rasul, G., Tong, J., Ali, G., Cheema, S.B., Liu, L., Gemmer, M., Fischer, T., 2015. Statistical downscaling and future scenario generation of temperatures for Pakistan Region. Theor. Appl. Climatol. 120 (1–2), 341–350.
Khadam, I.M., Kaluarachchi, J.J., 2004. Use of soft information to describe the relative uncertainty of calibration data in hydrologic models. Water Resour. Res. 40 (11).
Kim, J., Ivanov, V.Y., Fatichi, S., 2015. Climate change and uncertainty assessment over a hydroclimatic transect of Michigan. Stochastic Environ. Res. Risk Assess. 1–22.
Knutti, R., Sedláček, J., 2013. Robustness and uncertainties in the new CMIP5 climate model projections. Nat. Clim. Change 3 (4), 369–373.
Kundzewicz, Z., Mata, L., Arnell, N.W., Döll, P., Jimenez, B., Miller, K., Oki, T., Şen, Z., Shiklomanov, I., 2008. The implications of projected climate change for freshwater resources and their management.
Lee, J.H., Kim, C.J., 2013. A multimodel assessment of the climate change effect on the drought severity–duration–frequency relationship. Hydrol. Process. 27 (19), 2800–2813.
Liu, Y., Hwang, Y., 2015. Improving drought predictability in Arkansas using the ensemble PDSI forecast technique. Stochastic Environ. Res. Risk Assess. 29 (1), 79–91.
Loukas, A., Vasiliades, L., 2004. Probabilistic analysis of drought spatiotemporal characteristics in Thessaly region, Greece. Nat. Hazards Earth Syst. Sci. 4 (5/6), 719–731.
McKee, T.B., Doesken, N.J., Kleist, J., 1993. The relationship of drought frequency and duration to time scales. In: Proceedings of the 8th Conference on Applied Climatology. American Meteorological Society, Boston, MA, USA, pp. 179–183.
Menon, A., Levermann, A., Schewe, J., Lehmann, J., Frieler, K., 2013. Consistent increase in Indian monsoon rainfall and its variability across CMIP-5 models. Earth Syst. Dyn. 4 (2), 287–300. https://doi.org/10.5194/esd-4-287-2013.
Mishra, A., Desai, V., 2005. Spatial and temporal drought analysis in the Kansabati river basin, India. Int. J. River Basin Manage. 3 (1), 31–41.
Mishra, A., Singh, V.P., 2009. Analysis of drought severity-area-frequency curves using a general circulation model and scenario uncertainty. J. Geophys. Res.: Atmos. 114 (D6).
Mishra, V., Cherkauer, K.A., 2010. Retrospective droughts in the crop growing season: implications to corn and soybean yield in the Midwestern United States. Agric. For. Meteorol. 150 (7–8), 1030–1045. https://doi.org/10.1016/j.agrformet.2010.04.002.
Miyan, M.A., 2015. Droughts in Asian least developed countries: vulnerability and sustainability. Weather Clim. Extremes 7, 8–23.
Mullan, D., Chen, J., Zhang, X., 2015. Validation of non-stationary precipitation series for site-specific impact assessment: comparison of two statistical downscaling techniques. Clim. Dyn. https://doi.org/10.1007/s00382-015-2626-x.
Nam, W.-H., Hayes, M.J., Svoboda, M.D., Tadesse, T., Wilhite, D.A., 2015. Drought hazard assessment in the context of climate change for South Korea. Agric. Water Manage. 160, 106–117. https://doi.org/10.1016/j.agwat.2015.06.029.
Naz Mirza, S., Athar, M., Qayyum, M., 2009. Effect of drought on rangeland productivity and animal performance in dryland region of Balochistan, Pakistan. Agric. Conspectus Sci. (ACS) 74 (2), 105–109.
Ouyang, F., Zhu, Y., Fu, G., Lü, H., Zhang, A., Yu, Z., Chen, X., 2015. Impacts of climate change under CMIP5 RCP scenarios on streamflow in the Huangnizhuang catchment. Stochastic Environ. Res. Risk Assess. 29 (7), 1781–1795. https://doi.org/10.1007/s00477-014-1018-9.
Panofsky, H.A., Brier, G.W., Best, W.H., 1958. Some application of statistics to meteorology.
Rahmat, S.N., Jayasuriya, N., Bhuiyan, M.A., 2016. Short-term droughts forecast using Markov chain model in Victoria, Australia. Theor. Appl. Climatol. 129 (1–2), 445–457. https://doi.org/10.1007/s00704-016-1785-y.
Rajsekhar, D., Singh, V.P., Mishra, A.K., 2015. Integrated drought causality, hazard, and vulnerability assessment for future socioeconomic scenarios: an information theory perspective. J. Geophys. Res.: Atmos. 120 (13), 6346–6378.
Rashid, M.M., Beecham, S., Chowdhury, R.K., 2015. Statistical downscaling of CMIP5 outputs for projecting future changes in rainfall in the Onkaparinga catchment. Sci. Total Environ. 530, 171–182.
Rubin, D.B., 1981. The bayesian bootstrap. Ann. Stat. 9 (1), 130–134.
Sa'adi, Z., Shahid, S., Chung, E.-S., bin Ismail, T., 2017. Projection of spatial and temporal changes of rainfall in Sarawak of Borneo Island using statistical downscaling of CMIP5 models. Atmos. Res. 197, 446–460.
Sarwar, A., 2008. Droughts in Pakistan—A Socio-political. Perspective, Droughts and Integrated Water Resource Management in South Asia. SAGE Publications Pvt. Ltd.
Schneider, U., Becker, A., Finger, P., Meyer-Christoffer, A., Ziese, M., Rudolf, B., 2014. GPCC's new land surface precipitation climatology based on quality-controlled in situ data and its role in quantifying the global water cycle. Theor. Appl. Climatol. 115 (1–2), 15–40.
Shafiq, M., Kakar, M., 2007. Effects of drought on livestock sector in Balochistan Province of Pakistan. Int. J. Agric. Biol. (Pakistan).
Shirvani, A., Landman, W.A., 2015. Seasonal precipitation forecast skill over Iran. Int. J. Climatol. 36 (4), 1887–1900. https://doi.org/10.1002/joc.4467.
Snead, R.E., 1968. Weather patterns in Southern West Pakistan. Arch. Met. Geoph. Biokl. B. 16 (4), 316–346. https://doi.org/10.1007/bf02243179.
Spinoni, J., Naumann, G., Carrao, H., Barbosa, P., Vogt, J., 2014. World drought frequency, duration, and severity for 1951–2010. Int. J. Climatol. 34 (8), 2792–2804. https://doi.org/10.1002/joc.3875.
Swain, S., Hayhoe, K., 2015. CMIP5 projected changes in spring and summer drought and wet conditions over North America. Clim. Dyn. 44 (9–10), 2737–2750.
Taylor, I., Burke, E., McColl, L., Falloon, P., Harris, G., McNeall, D., 2013. The impact of climate mitigation on projections of future drought. Hydrol. Earth Syst. Sci 17, 2339–2358.
Touma, D., Ashfaq, M., Nayak, M.A., Kao, S.-C., Diffenbaugh, N.S., 2015. A multi-model and multi-index evaluation of drought characteristics in the 21st century. J. Hydrol. 526, 196–207. https://doi.org/10.1016/j.jhydrol.2014.12.011.
Van Vuuren, D.P., Edmonds, J., Kainuma, M., Riahi, K., Thomson, A., Hibbard, K., Hurtt, G.C., Kram, T., Krey, V., Lamarque, J.-F., 2011. The representative concentration pathways: an overview. Clim. Change 109 (1–2), 5.
Verheijen, O., 1998. Community Irrigation Systems in the Province of Balochistan. IWMI.
Vidal, J.P., Wade, S., 2009. A multimodel assessment of future climatological droughts in the United Kingdom. Int. J. Climatol. 29 (14), 2056–2071.
Villarini, G., Scoccimarro, E., White, K.D., Arnold, J.R., Schilling, K.E., Ghosh, J., 2015. Projected changes in discharge in an agricultural watershed in Iowa. JAWRA J. Am. Water Resour. Assoc. 51 (5), 1361–1371. https://doi.org/10.1111/1752-1688.12318.
Wang, L., Chen, W., 2014. A CMIP5 multimodel projection of future temperature, precipitation, and climatological drought in China. Int. J. Climatol. 34 (6), 2059–2078.
Wang, L., Chen, W., Zhou, W., 2014. Assessment of future drought in Southwest China based on CMIP5 multimodel projections. Adv. Atmos. Sci. 31 (5), 1035–1050.
Wang, X.-J., Jian-yun, Z., Shahid, S., ElMahdi, A., Rui-min, H., Zhen-xin, B., Ali, M., 2012. Water resources management strategy for adaptation to droughts in China. Mitigation Adapt. Strategies Global Change 17 (8), 923–937.
Wilby, R.L., Wigley, T., 1997. Downscaling general circulation model output: a review of methods and limitations. Prog. Phys. Geogr. 21 (4), 530–548.
Wilby, R.L., Wigley, T., Conway, D., Jones, P., Hewitson, B., Main, J., Wilks, D., 1998. Statistical downscaling of general circulation model output: a comparison of methods. Water Resour. Res. 34 (11), 2995–3008.
Winkler, T., Winiwarter, W., 2015. Greenhouse gas scenarios for Austria: a comparison of different approaches to emission trends. Mitigation Adapt. Strategies Global Change 1–16.
Yin, Y., Ma, D., Wu, S., Pan, T., 2015. Projections of aridity and its regional variability over China in the mid-21st century. Int. J. Climatol.
Zahid, M., Iqbal, W., 2015. Multi-model cropping seasons projections over Pakistan under representative concentration pathways. Model. Earth Syst. Environ. 1 (3), 1–12. https://doi.org/10.1007/s40808-015-0008-3.
Zahid, M., Rasul, G., 2012. Changing trends of thermal extremes in Pakistan. Clim. Change 113 (3–4), 883–896.
Zarch, M.A.A., Sivakumar, B., Sharma, A., 2015. Droughts in a warming climate: a global assessment of Standardized precipitation index (SPI) and Reconnaissance drought index (RDI). J. Hydrol. 526, 183–195.